

<https://doi.org/10.1038/s43247-025-02018-5>

Magmatic volatiles control the sub-plinian basaltic eruptions at Ambae volcano, Vanuatu

Check for updates

Philipson Bani ^{1,2}✉, Alessandro Aiuppa ³, Diego Coppola ⁴, Simon Carn ⁵, Dominique Cluzel ⁶, Estelle Rose-Koga ⁷, Etienne Medard ², François Nauret ², Yves Moussallam⁸, Dan Tari⁹ & Iuma Bani⁹

The 2017–2018 eruption of Ambae volcano provided a rare opportunity to investigate gas emissions during a sub-Plinian basaltic eruption. Here we document the gas emissions during this eruption using satellite observation, alongside gas measurements and geochemical analyses. Our results indicate that the volcano released 3.3 teragrams of sulfur dioxide, 7.7 of carbon dioxide, 134 of water vapour, 0.2 of hydrogen sulfide, and 0,001 of dihydrogen, ranking Ambae among the world's top volcanic gas emitters. Despite these substantial emissions, the relatively modest volume of 0.47 cubic kilometer of magma that fueled the eruption indicates a volatile-rich magma source. This enrichment is likely linked to the geodynamic setting, where subduction of the faulted, carbonate-rich D'Entrecasteaux Ridge, coupled with an influx of fertile mantle, fostered the formation of volatile-rich magma. High concentrations of volatiles, can drive substantial gas exsolution, increasing magma buoyancy, resulting in greater magma supply and faster ascent rates. Rapid ascent prevents volatile separation from the melt, resulting in powerful gas surges that drive the transition from effusive to basaltic sub-Plinian eruption phases.

Basaltic volcanoes are generally characterized by the effusive nature of their eruptions, associated with mild explosive events, such as lava fountaining and/or Strombolian explosions. The occurrence and intensity of these events are influenced by factors such as the degree of gas-melt decoupling, the magma ascent rate, and the extent of bubble coalescence within the magma^{1–3}. If magma ascent rate is high, bubble coalescence is minimized, leading to a high population of millimeter to centimeter size bubbles in the shallow conduit, ultimately sustaining a fountaining eruption^{3–5}. In contrast, with a slow rising magma, gas slugs can develop and migrate upward within the ascending melt to produce Strombolian explosions^{3–5}. These manifestations are thought to be induced by a low magma viscosity that generally inhibits fragmentation. Sub-Plinian to Plinian explosions are rare at basaltic volcanoes, but yet their occurrence is now documented at several volcanoes (e.g., ref. 6), including the 8.6 ka eruption of La Vache and Lassolas in the Chaîne des Puys⁷, the 2.2 ka eruption of Mt. Fuji (Japan), the 1125–1050 CE eruption of Sunset Crater

(Arizona, USA)⁸, the 1999 CE eruption of Shishaldin (Alaska, USA)^{9–11}, the 2.1 ka Masaya Triple Layer eruptions (Nicaragua)^{12–16}, the 122 BCE eruption of Etna (Italy)¹⁷ and the 1886 CE eruption of Tarawera (New Zealand)^{18,19}. These past basaltic Plinian events have been studied mainly by investigating their tephra deposits and modeling. The gas emissions associated with these past events miss precise estimation. Therefore, the 2017–2018 eruption of Ambae, in the Vanuatu archipelago, stands out as a rare example of witnessed sub-Plinian or Plinian basaltic event. Here we provide a comprehensively characterization of this eruption, by presenting its gas emissions and surface thermal heat flux. This is combined with the chemistry of bulk rocks and melt inclusions from our previous study²⁰, now supplemented with bulk rock chemistry of phase 4, which was not included in our 2019 work. By comprehensive examination of these datasets, we attempt at shedding light into the potential processes that culminated in the observed sub-Plinian eruption, with an emphasis on the role of volatile content and surface degassing.

¹Centre IRD de la Nouvelle-Calédonie, 101, Promenade Roger Laroque, BP A5, 98848 Nouméa Cedex, Nouvelle-Calédonie. ²Laboratoire Magmas et Volcans, Université Blaise Pascal-CNRS-IRD, OPGC, 63170 Aubière, France. ³Università degli Studi di Palermo, Dipartimento di Scienze della Terra e del mare, Palermo, Italy. ⁴Dipartimento Di Scienze Della Terra, Università Di Torino, Torino, Italy. ⁵Department of Geological and Mining Engineering and Sciences, Michigan Technological University, Houghton, MI, 49931, USA. ⁶Institut de Sciences Exactes et Appliquées, Université de la Nouvelle-Calédonie, BP R4, 98851 Nouméa Cedex, New Caledonia. ⁷Institut Des Sciences de La Terre d'Orleans (ISTO), UO/CNRS/BRGM, 1A Rue de La Ferrollerie, 45071 Orleans, France. ⁸Lamont-Doherty Earth Observatory, Columbia University, New York, NY, 10027, USA. ⁹Vanuatu Meteorology and Geohazards Department, Port Vila, Vanuatu.

✉e-mail: philipson.bani@ird.fr

The 2017–2018 eruption of Ambae

The short chronology of Ambae's volcanic activity is summarized in ref. 21 and amended in Table 1. The volcanic activity on Ambae resumed in the early 1990s after more than 300 years of dormancy. Gradually, the Crater Lake Voui became acidic and the gaseous emanation through the lake destroyed the lush forest, first on the lake's islets and then around the crater^{22,23}. The first eruptive manifestation was a phreatic event (Table 1) which peaked in March 1995²² when meter-size bubbles at the surface of the $40 \times 10^6 \text{ m}^3$ of Voui crater lake²³ were observed and a gray ashy-column was seen rising above the summit of Ambae volcano²². Ten years later, in 2005, a sustained surtseyan eruption was observed^{21,24} that lasted a month and a half, from end-November 2005 to mid-January 2006^{21,25}. The area around the Voui crater lake was extensively covered by ash but no impact was reported along the coast where the majority of the island's population live. Five months later, in June 2006, the color of Voui Lake water entirely changed from blue to red in response to ion oxidation²¹.

The 2017–2018 eruption, the subject of this work, is the third eruptive event at Ambae since activity resumption. This major event lasted a whole year, from September 2017 to August 2018. The activity went through 4 distinct intense eruptive phases, separated by episodes of relative calm phase as summarized in Table 1. The first intense manifestation (phase 1) was the onset of the eruption, from September 5–10, 2017. Large explosions on September 6 released about 38 kilotons (kt) of SO_2 , measured by the (Ozone Monitoring Instrument (OMI) on NASA's Aura satellite (<https://so2.gsfc.nasa.gov>). The activity then became relatively quiet between September 10 and 21. During a visit to the summit on October 17, 2017, a large block exceeding 3 m^3 was found at about one kilometer away from the active vent with a large impact crater on the ground. No other rock of this size was found beyond the rim during the later phases of the eruption. The second strong eruption phase (phase 2) commenced around September 22, 2017, when the Moderate Resolution Imaging Spectroradiometer (MODIS) thermal alerts detected the first and very high thermal anomaly induced by a lava outburst in Voui crater (<http://modis.higp.hawaii.edu/>; www.mirovaweb.it). Local people who ventured to the summit during this period reported the lava fountaining activity. Aerial observations made on October 3 and October 6 confirmed the presence of lava flowing out at the base of a new cone, while at least three vents maintained strombolian activity at the top. The high thermal energy associated with phase 2 persisted until November 9, 2017, whilst SO_2 emissions were extremely high from October 14 to November 23, 2017, when eruption phase 2 ended. The strongest daily SO_2 emission reached 39 kt (October 22), while the highest Volcanic Radiative Power (VRP) of 2270 MW was recorded on November 5. From end-November 2017 to early-January 2018, there was a lull in eruptive activity. No thermal anomalies were observed and SO_2 emissions were relatively modest compared to the prior strong outgassing phases. The strong eruption phase 3 started around January 4, 2018 with an intense lava fountaining, but no lava flow, observed during a field survey. In contrast to phase 2, only intermittent thermal anomalies were observed during this phase. The highest thermal energy (912 MW) was observed on March 5, 2018, about 14 days before a period of intense eruptive degassing that lasted from March 19 to April 14. The maximum daily SO_2 release from this phase was 101 kt on April 6. Phase 3 lasted approximately 3 months and ended on April 14. It was followed by another lull in activity from mid-April to mid-June 2018. The intense eruption phase 4 commenced on June 21 with the occurrence of strong thermal energy at the surface. In contrast to early phases, the thermal energy was relatively small. The highest thermal energy release during this phase was recorded on July 7 (353 MW) just 10 days before the extreme eruptive degassing that lasted between July 17 and August 3, 2018. During this period, the maximum daily SO_2 output peaked at ~ 390 kt, the highest of the entire eruption (Fig. 1; Supplementary clip 1).

This succession of intense eruptive periods and lulls has strongly challenged the volcanic risk management during the crises. Two distinct evacuations of the 11,000 inhabitants of Ambae were carried out. About 2/3 of the island's vegetation was damaged by acid rain and heavy ash fall. Ash deposits about one meter thickness were observed in the caldera at the top of

the volcano, while along the coast, ash deposits of 1 to 2 centimeters were reported. Several buildings collapsed due to the weight of the ash deposits. Numerous lahars have been reported during and after the crisis and the transported materials have transformed the rocky coasts into wide black sand beaches²⁶. The most destructive lahar occurred during the night of 30–31 March 2018 at 1–2 am. It swept away an entire village called Waluembue. By chance, the event occurred in two phases. The first, relatively small flow forced the inhabitants to flee their houses, just before the 2nd flow, which occurred half an hour later that swept away all the houses in its path²⁶. Despite the intensity and long duration of the eruptive event, only two direct victims were reported, and both were killed by lahars.

Results

Very high levels of SO_2 emitted during the Ambae eruption in 2017–2018

Residents of Ambae witnessed the first explosions on September 5, and by September 6, 2017, OMI satellite data indicated the presence of ~ 38 kt SO_2 over Ambae (Table 2). This substantial sulfurous cloud over Ambae was a surprise because such a large amount had never been documented on this particular volcano. SO_2 emissions then gradually decreased to background levels over the next 3 days. The total mass of SO_2 discharged over this period of extreme degassing (hereafter referred to as Extreme Degassing Period 1, EDP1) is 76 kt (Fig. 2, Table 2). Two series of airborne DOAS (Differential Optical Absorption Spectroscopy) traverses and scanning measurements carried out after this first extreme degassing (Supplementary table 1) indicate a mean SO_2 flux fluctuating between 350 ± 120 t/d on the October 3 and $>5500 \pm 1700$ t/d on October 6, 2017. The former value is comparable to the satellite estimate (292 t, Fig. 2) but likely underestimates the SO_2 emission rate since the scanning profiles are only partially completed. A month later, after this first intense SO_2 emission, satellite observations revealed another period of extreme SO_2 release (EDP2) which commenced on October 14 and persisted until November 23, 2017. This time satellites measured a gradual increase from >11 kt on October 14 to a maximum of >39 kt on October 22, 2017. For nearly a month and a half, more than 516 kt of SO_2 were injected into the atmosphere at an average daily emission rate of 16 kt/d (Table 2). This 2nd extreme degassing phase was followed by 3.5 months of relative calm with persistent strong degassing, characterized by an average daily SO_2 output of >4 kt. On March 19, 2018, a third period of extreme SO_2 degassing (EDP3) began with ~ 8 kt measured above the volcano. Over the following weeks, emissions steadily increased, peaking at over 101 kt on April 6, 2018. Emissions then dropped to background levels by April 14, 2018. This third extreme degassing phase lasted nearly 4 weeks and resulted in a total release of 945 kt of SO_2 , with a daily average of >36 kt. For three months after this third extreme degassing, Ambae experienced a period of relative calm during which the average daily SO_2 output dropped to a mean value of ~ 2 kt. This relative calm ended on July 17 when the fourth and most intense eruption phase (EDP4) started. EDP4 released a total of 1074 kt of SO_2 into the atmosphere with a daily average of 72 kt. The maximum daily SO_2 mass was 390 kt, measured by Tropospheric Monitoring Instrument (TROPOMI) on July 28, 2018 (Fig. 1). This was the largest single emission of the entire 2017–2018 eruption, and included large stratospheric injection of SO_2 ²⁷. EDP4 lasted only 17 days, ending on August 3, 2018 and marking the end of a year-long period of eruptive activity. The cumulative mass of SO_2 released during the four phases of extreme degassing totals up to 2.6 ± 0.4 Tg. When the emissions from relative calm phases are also taken into account, the total SO_2 released into the atmosphere during the Ambae 2017–2018 eruption increases to 3.3 ± 0.2 Tg of SO_2 (Fig. 2). This figure exceeds the SO_2 released by several Volcanic Explosivity Index (VEI) 4 eruptions, such as the 1982–1983 Galunggung eruption (Java, Indonesia) or the Kasatochi eruption (Alaska, USA) in 2008²⁸ (Fig. 2). If emissions from the 4 most intense eruptive phases are considered separately, one can observe that EDP3 and EDP4 released more SO_2 than the VEI 3 eruptions of Nevado del Ruiz (0.66 Tg, 1985) and Redoubt (0.61 Tg, 2009), whilst the SO_2 discharge by EDP2 is higher than that from the VEI 4 eruption of Merapi (0.44 Tg, 2010) (Fig. 2). Even EDP1 released more SO_2 than the VEI

Table 1 | Chronology of Ambae’s volcanic activity from ref. 21 with details on the 2017–2018 eruption (this work)

~1575 ± 54		Explosion at the summit and formation of the Voui cone and the Manaro Ngoru crater
~1670		Fissural eruption on the western flank, along N50 fractures, damaging the Ndui Ndui region. Formation of a palagonitic tuf cone in the lake Voui.
1870 ± 1		Lahar event causing victims.
~1916		Eruption? (and/or earthquake) triggering a landslide killing about 100 people.
1966		Vapour emission, strong fumarole activity.
1971		Strong vapour emission
1976		Strong activity on Solfatara
1991		On the 13 of July — 3 boiled zones identified in lake Voui and acid impact on vegetation on Voui crater rim.
1993		Increase of vegetation damage around Voui.
1994		On the 4th and 5th December large quakes were felt on the island.
1995		On the 3rd of March ash plume was seen. High tremor recorded, high degassing from lake Voui.
2005–2006		Surtseyan eruption and spectacular colour change in lake Voui
2017–2018 eruption		
Eruption phase 1	September 5–10, 2017	A large explosion at the summit was heard up to 10 km away from the Ambae summit (September 5). It marked the onset of the eruptive event. A large quantity of SO ₂ (38 kt) was detected by the OMI above the Ambae volcano during the following days. The activity alert level raised from 2 (major unrest) to 3 (minor eruption), following the Vanuatu Volcanic Alert Level System (VVALS).
Relative calm phase	September 10–21, 2017	A short period of relative calm followed the onset event. During this period the gas emission returned to its background level.
Eruption phase 2	September 22–November 23, 2017	<p>On September 22, 2017, MODIS detected the first thermal anomaly with a very high thermal energy release (318 MW) within Lake Voui (September 22). Inhabitants have reported the appearance of a sustained glow at the summit in relation to the new lava flow on Ambae after that of Ndundui, some ~350 years ago. The activity alert level was raised from 3 to 4 (moderate eruption — according to VVALS) on September 23.</p> <p>On September 25, 2017, the national Government imposed the first state of emergency, prompting the evacuation of the entire population of the island. Lava flows continued in the Voui crater.</p> <p>On October 3, 2017, observation flight confirmed the sustained eruptive activity, which was restricted to the crater lake Voui. A lava flow continued to spread from a well formed cone and a strombolian manifestation was observed on 3 active vents.</p> <p>On October 6, 2017, another observation flight confirmed a continuous eruption but with no further increase, in comparison to the October 3 observation. The eruptive activity alert level downgraded from 4 to 3.</p> <p>From October 10 to November 23, 2017, lava continued to flow from the new cone; another period of large SO₂ release was recorded by satellites, mainly from October 14 to November 23. A field survey at the summit on the October 17 confirmed this persistent strong degassing sustained by a strombolian activity. MODIS thermal alert, which was issued continuously since September 22 in relation to lava flow and strombolian activity, has ceased on November 9, although an alert with less thermal energy was issued on November 17. The 1st state of Emergency ended on October 27, allowing the population to return. However on their return, they found themselves exposed to stronger eruptive manifestations in comparison to that of September. Ash deposits reached the coast whilst acid rain devastated the vegetation to the north-west and western part of the island. Crops were destroyed and drinking water reservoirs were contaminated.</p>
Relative calm phase	November 24, 2017–early January 3, 2018	A relative calm was observed from end November 2017 to early January 2018. MODIS thermal alert ceased and no ash fall was observed. Gas emission reduced to near background level. Volcanic activity level downgraded to 2 (December 7). A field survey at the summit (January 5), confirmed that lava flow had stopped.
Eruption phase 3	January 4–April 11, 2018	A new strong thermal energy release (368 MW) occurred on January 4, which marked the beginning of the eruption phase 3. It persisted until April 11. The SO ₂ emission exhibited another extreme degassing phase from March 19 to April 14. Heavy ash falls were witnessed, especially towards the northern and southern parts of the island. On 6 April, residents living in the north-western area witnessed a short nightfall at about midday. Due to cyclone Hola (March 6–7) many lahars have occurred. A village (Waluebue) in the northern part of Ambae was destroyed by a lahar during the night of 30 March 2018. The alert level was again raised to 3 on April 4.
Relative calm phase	April 15–June 20, 2018	No ash fall and acidic rainfall reported. A field survey at the summit on May 23, confirmed the lull of activity. The summit was covered with ash deposits, that were up to almost a meter thick in some places. The lake was divided into two parts by the newly-formed cone and in both parts the water was red. It was possible to reach the rim of this new cone for gas measurements. On June 7, the alert level was downgraded to 2.
Eruption phase 4	June 21–August 4, 2018	A new and more powerful eruptive activity was witnessed. It commenced on June 21 with a thermal alert and followed by an extreme degassing phase that started on July 17. Heavy ash falls caused a nightfall at mid-day on July 25 ³² . Houses collapsed under overload of ash. The alert level was raised to 4 (July 21), and a 2nd state of emergency was issued (July 26). The whole population was again evacuated from the island. The strong degassing ceased on August 3 while the last thermal alert was released earlier, on July 26. This final violent event lasted about 2 weeks and was the final phase of this year-long eruptive activity.

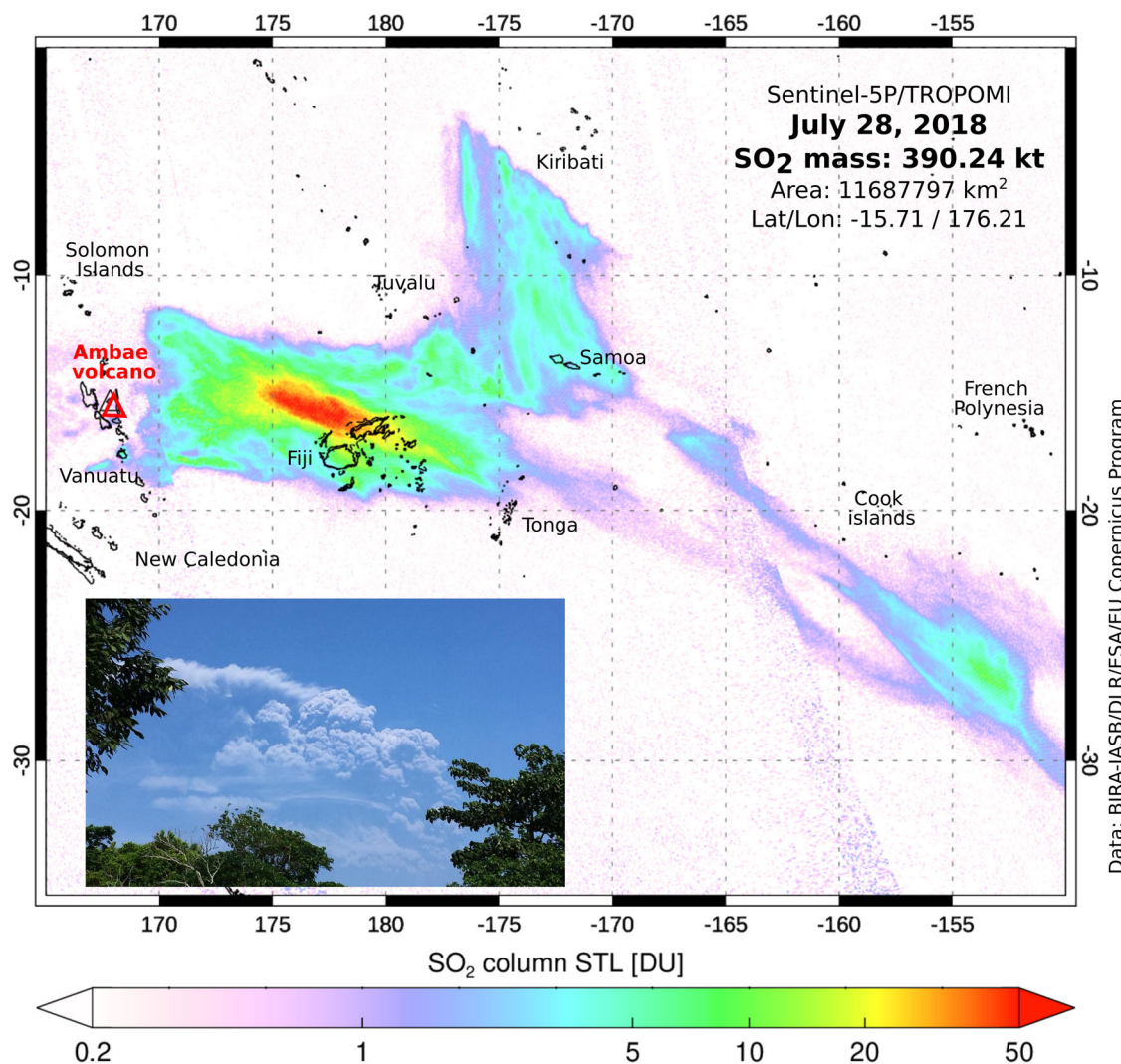


Fig. 1 | Ambae Eruption: Over 390 kt of SO₂ dispersed across 4000 km in the South Pacific. More than 390 kt of SO₂ were measured during the most intense eruptive phase of Ambae, dispersing across numerous South Pacific countries over a

distance of 4,000 kilometers from the source. The thumbnail shows the eruptive column of July 27, 2018—photo courtesy, Veronica Legler / Peace Corps Vanuatu.

3 eruption of Anathan (0.07 Tg, 2005). Therefore, Ambae stands out as one of the largest contributors of eruptive SO₂ to the atmosphere, and may rank 6th according to the list compiled for eruptive contributions in the period 1978–2014²⁸.

A CO₂-rich magmatic system

The gas composition of Ambae had never been measured before this work, partly because most of the volcanic gas dissolved into the 40×10^6 m³ of water of the crater lake of Voui²³, before the 2017–2018 eruption. The process has maintained a very high acidity level of the Voui Lake²¹. However, during the first two phases of the eruption, successive lava flows and tephra deposits led to the formation of a new cone of about 1 km in diameter and 150 m high. When reaching the summit on May 2018 (this work), the new cone had a crater of ~300 m in diameter, through which magmatic gas escaped directly into the atmosphere. Only a limited period of time was spent on the rim of this cone, due to the high level of activity, to record the gas composition of this volcano for the first time ever. Our Multi-GAS derived in-plume concentration time series, presented in Fig. 3, exhibit a good correlation between the SO₂ and other measured gas species, suggesting a common magmatic source. The derived gas to SO₂ ratios are 60–260, 0.10–0.12, 1.6–5.3 and 0.01–0.02 for H₂O/SO₂, H₂S/SO₂, CO₂/SO₂ and H₂/SO₂ respectively (Table 3). The range of CO₂/SO₂ ratios observed likely reflect distinct

compositions for the several vents active inside the crater at the time of our survey. Assuming that the averaged ratios are representative of the system, then the magmatic gas composition of Ambae is inferred at 97 mol.% H₂O, 2 mol.% CO₂, 0.7 mol.% SO₂, 0.07 mol.% H₂S and 0.01 mol.% H₂ (Table 3). Scaling these gas ratios to the amount of SO₂ obtained from satellite data (3.3 Mt) yields the equivalent of 134 ± 4 Mt of H₂O, 7.7 ± 0.2 Mt of CO₂, $0.2 \pm 6E-3$ Mt of H₂S, and $0.001 \pm 4E-5$ Mt of H₂ (Table 3) for the entire eruptive period, which is a considerable contribution to the atmosphere. The total CO₂ released is substantial for a single volcano, comparable for instance to the annual CO₂ budget passively released each year from all South America volcanoes (6.4 Mt)²⁹, and represents ~20% of the global CO₂ from active volcanoes through passive degassing (39 Mt/yr)³⁰. Hence, Ambae can be considered as a notable CO₂ source. The CO₂/S_T ratios (S_T being the sum of SO₂ and H₂S) of Ambae gas fluctuates between 1.4 and 4.7 (Table 3) and plot at the upper range of the arc volcanism representative field in the H₂O–CO₂–S_T ternary diagram (Fig. 3). This CO₂-rich character of the Ambae gas is in contrast with observations made at other volcanoes of the Vanuatu arc (Mount Garet, Ambrym, Yasur) that display low-carbon gas^{31–33} (Fig. 3). However, this Ambae gas composition overlaps with that of Merapi, and is close to that of Bromo, two Indonesian volcanoes fueled by volatile-rich sources derived from dehydration of a subducting slab containing carbon-enriched subducted sediments^{34,35}. Therefore, our results

Table 2 | Total of recorded SO₂ mass break down into eruptive phases

Satellite SO ₂ measurements during during the Ambae 2017–2018 eruption							
Periods	EDP1 September 5–10, 2017 (6 days)—P1	Rel calm phase September 11–October 13, 2017 (33 days)	EDP2 October 14–November 23, 2017 (41 days)	Relative calm phase November 24, 2017–March 18, 2018 (115 days)	EDP3 March 19–April 14, 2018 (27 days)	Relative calm phase April 15–July 16, 2018 (93 days)	EDP 4 July 17–August 03, 2018 (18 days)
Min. daily value (kt)	0,7	0,3	0,4	0,2	2,1	0,07	5,6
Max. daily value (kt)	38,1	4,8	39,1	19,2	101,3	15,0	390,0
Mean daily value (kt)	15,2	1,8	16,1	4,7	36,3	2,1	71,6
Cumulative value (kt)	76.1	57,2	516,3	470.0	944,8	177,5	1074,4
Standard dev.	15,4	1,2	12.0	4.0	26,7	2,7	92,8
Total SO₂ released during eruption: 3316 ± 155 kt (3.3 ± 0.2 Tg)							

suggest that combination of (1) the magma source that fueled the Ambae eruption being enriched in CO₂, and (2) the magmatic gas that sustained the eruption being separated at depth in the plumbing system (hence resulting CO₂-enriched), as highlighted by the CO₂-SO₂-H₂S ternary plot (Fig. 3). A deep and CO₂-enriched source is also supported by melt inclusions (Fig. 3, Supplementary Table 2, and see complete dataset in ref. 20), that show elevated CO₂ contents (up to >3800 ppm), relative to volatile contents in basalts from other subduction zones (from ref. 36). The CO₂ versus H₂O diagram for Ambae inclusions shows that the most elevated CO₂ levels were observed in EDP1 samples (>3800 ppm). CO₂ contents then decreased to ~2000 ppm in EDP2, and to <1000 ppm in EDP3 and possibly EDP4 (Fig. 3), indicating eruption of more shallowly stored magma. The absence of melt inclusion analysis for Phase 4 necessitates the assumption that its volatile contents are comparable to those of Phase 3. This assumption is supported by several factors, including the comparable eruptive intensity, the duration of eruptive discharges, the quantity of SO₂ emitted, and the bulk compositions of tephra deposits, which collectively suggest analogous magmatic conditions. In any case, the above results support the idea that Ambae volcanic activity is in part sustained by a carbon-rich source, having a CO₂/S_T ratio greater than 4, following the classification in ref. 37. Two mechanisms may possibly contribute to this high CO₂ source, including the subduction of ~650 m sediments with enriched carbonate content³⁸, carried by the d'Entrecasteaux Ridge³⁹, in front of Ambae volcano; and the westward and upward invasion of Indian Ocean-type MORB mantle (IOTMM) in the central part of Vanuatu and more particularly beneath Ambae, in response to the opening of the north Fiji basin⁴⁰ and the effect of buoyant ridge subduction⁴⁰. The IOTMM is an enriched mantle source^{40,41} that cannot be interpreted as induced by the DER input into the mantle wedge since the isotopic signatures point to a long term (>500 Ma) enrichment processes⁴¹. The proportion of CO₂ contributions from these two sources remains to be determined. Furthermore, this result should be used with caution, because no gas composition measurements have been conducted outside of the eruption period.

Lava discharge volume decreased over the eruption period

MODIS thermal alerts (MODVOLC; <http://modis.higp.hawaii.edu/>) and MIROVA (Middle Infrared Observations of Volcanic Activity—<https://www.mirovaweb.it/>) are widely recognized tools for volcano monitoring, particularly during volcanic crises^{42,43}. In the case of the 2017–2018 Ambae eruption, they provided a valuable means to monitor the activity. The first thermal alert of the 2017–2018 eruption was issued on September 22, 2017 with a VRP of 457 MW, and during the whole eruption period MIROVA recorded 102 thermal alerts distributed into three distinct phases. The first phase, which ran from September 22 to November 9 (hereafter referred to as

Thermal Radiation Phase 1 or TRP1), was the most energetic, emphasized by three significant VRP pulses, including 1424 MW on October 1, 883 MW on October 19 and 2270 MW on November 5, 2017. The second phase of thermal activity (TRP2) was observed between January 4 and April 11, 2018. This is the longest period of thermal manifestations at the surface, but in contrast to TRP1, was characterized by more intermittent thermal release behavior. The maximum VRP value of 912 MW was measured on March 5, 2018. The third and final period of thermal manifestation (TRP3) was observed between June 21 and July 26, 2018. This is the shortest period of thermal activity with a maximum VRP value of only 353 MW on July 7, 2018. The cumulated lava volume erupted at the surface, obtained following the approach of ref. 44 highlights a high mean extrusion rate of $4.3 \times 10^5 \text{ m}^3/\text{d}$ (~5 m³/s) in TRP1, which then fell to $8.8 \times 10^4 \text{ m}^3/\text{d}$ (~1 m³/s) in TRP2, and then to $1.2 \times 10^5 \text{ m}^3/\text{d}$ (~1 m³/s) in TRP3. The strongest mean discharge rate during TRP1 corresponds to the period of lava fountaining, lava flow and strombolian activity. TRP2 and TRP3 periods were sustained by lava fountaining, strombolian activity and explosive discharges. The cumulative discharged volume for the whole eruption period amounts to 0.034 km³ with a lower and upper bounds of 0.016 and 0.050 km³ respectively (Supplementary Fig. 1).

Transition to a more primitive basaltic source

The bulk compositions of the tephra samples collected during the four strong eruption phases are presented in Supplementary Table 2. The SiO₂ vs. total alkali plot (Fig. 4) shows a transition from a basaltic andesite composition in EDP1 to a composition intermediate between basalt and trachy-basalt composition in EDP2 and EDP3, and finally to a more primitive basaltic composition during EDP4. This large range of SiO₂ content (47.8–54.8 wt. %) in the 2017–2018 eruptive products contrasts with past eruptions that show bulk rock compositions restricted to basalts (Fig. 4). The highest SiO₂ content of 2017–2018 eruption corresponds to a large block that fell about a kilometer from the active vent during the onset phase. In terms of alkali content, samples from 2017 to 2018 event are relatively more alkali-rich than previous eruptions, with the exception of the samples from phase 1 that plot well below the alkaline/sub-alkaline line. The Harker diagrams, drawn relative to MgO content (Fig. 4), point to high Na₂O (2.48–3.51 wt. %), K₂O (1.56–1.90 wt. %) and low CaO (9.22–10.21 wt. %) compared to data from past works. The Fe₂O₃ content from the 2017–2018 eruption (9.70–10.34 wt. %) is in the lower range of past eruptions while the Al₂O₃ content varies in a narrow range (14.21–16.78%). The MgO content in our samples has a relatively narrow range (5.17–10.23 wt. %), compare to past data, but display a relative increase from EDP1 to EDP4, paralleled by a decreasing trend of Na₂O, Al₂O₃, SiO₂, TiO₂ and K₂O (Fig. 4). Such a trend may indicate that deeper magma source gradually reached the surface over

the course of the eruption, as evidenced by melt inclusion results (Fig. 3). Trace elements (Supplementary Table 2) show a typical arc magma signature, with enrichment in highly incompatible elements (e.g., Ba contents range from 400 to 600 ppm), and negative Nb anomalies (Fig. 4). The flat

MREE to HREE (Sm/Yb between 1.84 to 2.91) patterns suggest that residual garnet was not present in the mantle source. All the trace element patterns are similar. In terms of ratios, Ba/Th, Ba/Nb and Zr/Nb correspond respectively to 197–223, 313–335, 40–42 for EDP1, to 236–238, 201–325,

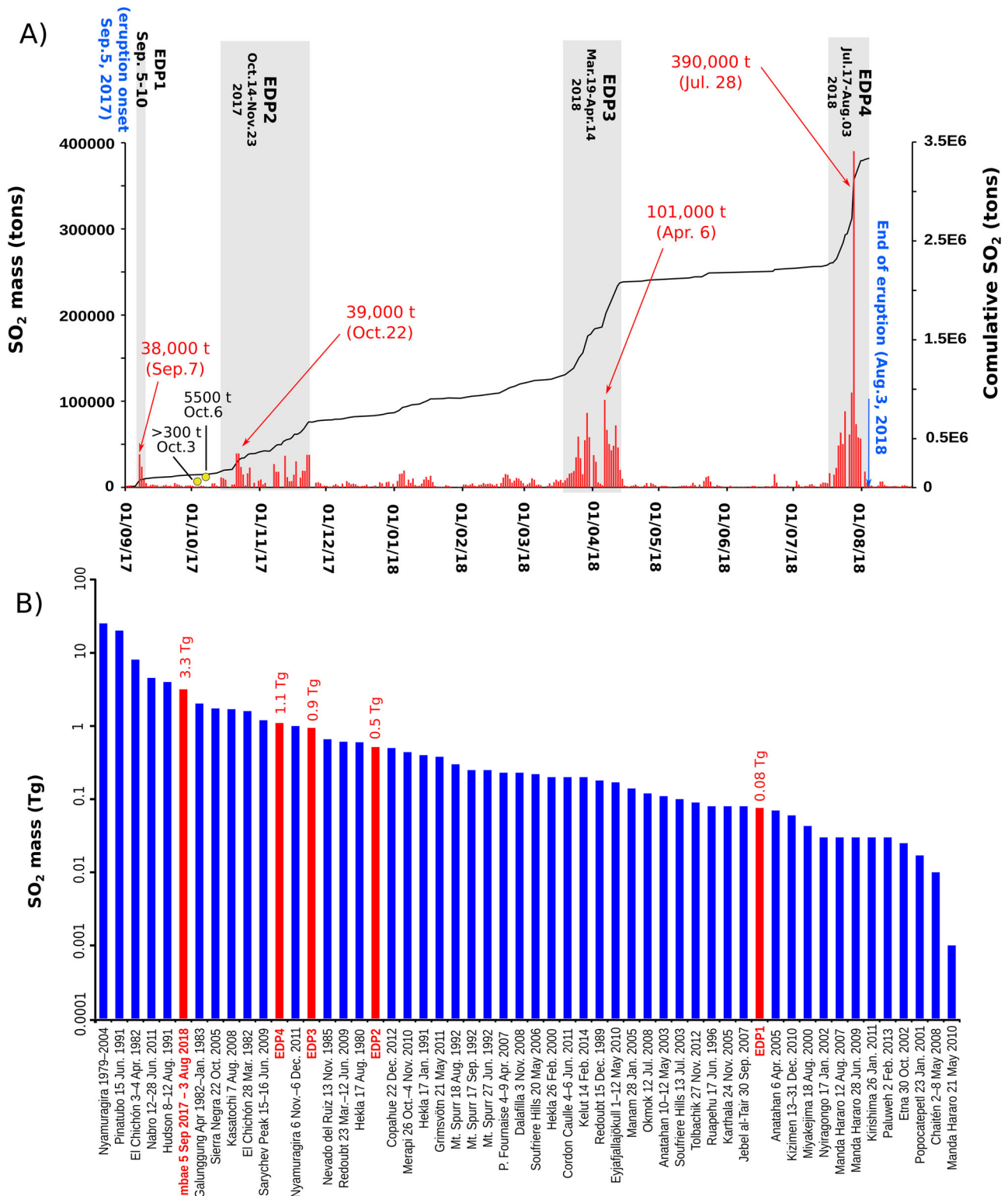
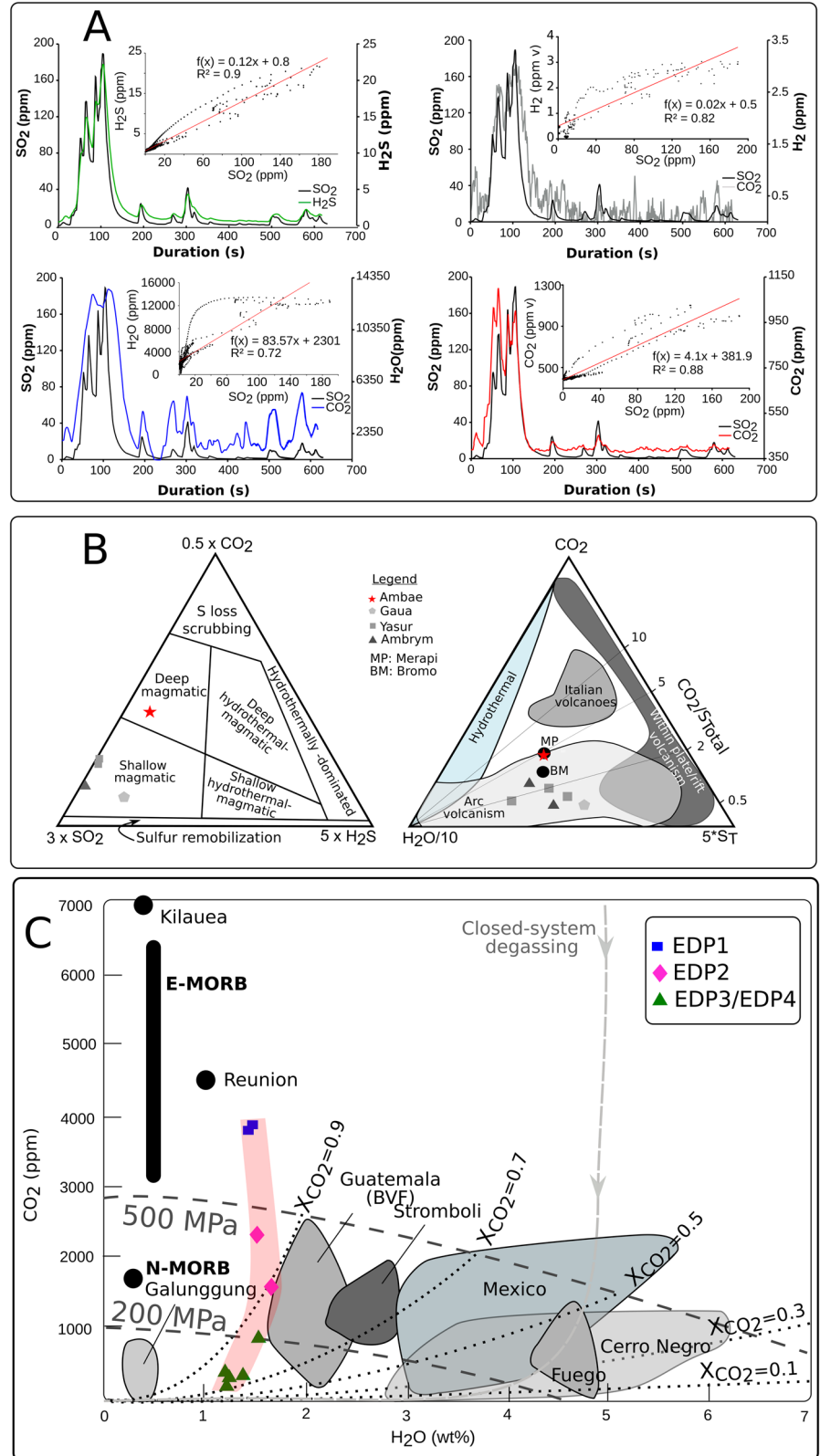


Fig. 2 | SO₂ emissions from Ambae eruption: daily discharge trends and comparative analysis. **A** Daily SO₂ mass recorded over Ambae during the whole eruptive period. The 4 phases of strong SO₂ discharge are highlighted and identified as EDP1, EDP2, EDP3 and EDP4. The maximum daily value for each phase is indicated (in red). The curve corresponds to the cumulative SO₂ values over the entire eruption

period and highlights the gradual increase in SO₂ discharge from EDP1 to EDP4, EDP1 being the onset eruptive discharge. The two yellow points correspond to the only DOAS SO₂ flux results. **B** The largest SO₂ loading per eruption in the period of 1978–2014²⁸. The contributions from the four eruptive phases and the total SO₂ released by the Ambae 2017–2018 eruption are shown in red.

Fig. 3 | Gas compositions and melt inclusions reveal a transition from deep to shallow magmatic carbon-rich sources beneath Ambae during the eruption. **A** Fluctuation of gas concentrations recorded on the rim of the new cone developed during the Ambae eruption. The correlations of the measured gases to SO₂ are provided. **B** Ternary diagrams showing a deep to shallow magmatic carbon-rich source beneath Ambae in comparison to other volcanoes of the Vanuatu arc. The CO₂-SO₂-H₂S diagram is adapted from ref. 83,84, while the CO₂-H₂O-S_T diagram is adapted ref. 33. The data sources include ref. 33 for Gaua, ref. 30 for Ambrym, ref. 31 for Yasur, ref. 34,35 for Merapi and Bromo, and the present study for Ambae. **C** Comparing the maximum CO₂ versus H₂O content from Ambae inclusions with inclusions in basalt from various subduction zones. The diagram is adapted from ref. 35, with sourced from ref. 36,85 and other references therein. The pink shaded zone highlights the decreasing trend in CO₂ levels throughout the eruptive event, indicating a progressive reduction in CO₂ contributions from a relatively deep source (>16 km) during EDP1, transitioning to ~10 km in EDP2, and ultimately approaching the surface in EDP3. This gradual decline occurred alongside a relatively modest but consistent H₂O content, which remained stable until the shallower depths of EDP3.



26–40 for EDP2, to 230–574, 215–291, 27–39 for EDP3 and to 259–301, 191–301, 28–39 for EDP4. These ratios are in the range of subduction zones (0.1–100) for Zr/Nb, whilst relatively higher for Ba/Th and Ba/Nb which may suggest fluid contributions from the subducted sediments and subducted slab (e.g. ref. 45). The volatiles from melt inclusions results (Supplementary Table 2; ref. 20) indicate strong variations in CO₂, S, Cl and F, as highlighted in ref. 20, with, respectively, 24–3899 ppm, 440–980 ppm,

1878–7243 ppm, 558–717 ppm in EDP1, similarly 12–2353 ppm, 208–1541 ppm, 2176–5348 ppm and 492–711 ppm in EDP2, and 8–946 ppm, 152–1183 ppm, 1435–3957 ppm, and 393–622 ppm for EDP3. Many processes can contribute to this wide range of volatile concentrations, including degassing and gas loss, crystallization, or post entrapment processes¹⁶. However, as noted in ref. 20, crystallization is unlikely to be the primary factor driving these fluctuations. Assuming that the highest

Table 3 | Gas composition and total degassing budget obtained by combining MultiGAS and satellite data

Gas concentration (ppm v)		Gas ratio		Gas composition				
Range		Range		Mean value	mol. %			
H₂O	9000–19000	H ₂ O/SO ₂	60–260	144	H ₂ O	96.95		
CO₂	390–1110	CO ₂ /SO ₂	1.6–5.3	3.4	CO ₂	2.29		
SO₂	0.06–220	H ₂ S/SO ₂	0.10–0.12	0.11	SO ₂	0.67		
H₂S	0.2–22	H ₂ /SO ₂	0.011–0.017	0.014	H ₂ S	0.07		
H₂	0.3–3	CO ₂ /S _T	1.4–4.7	2.8	H ₂	0.01		
EDP1 (kt)	Rel. Calm 1* (kt)	EDP2 (kt)	Rel. Calm 2* (kt)	EDP3 (kt)	Rel. Calm 3* (kt)	EDP 4 (kt)	Total (Mt)	
H₂O	3082	2317	20910	19035	38264	7188.7	43513.2	134 ± 4
CO₂	177.9	133.7	1206.8	1098.8	2208.5	414.9	2511.4	7.7 ± 0.2
SO₂	76.1	57.2	516.3	470.0	944.8	177.5	1074.4	3.3 ± 0.2
H₂S	4.4	3.3	30.2	27.5	55.2	10.4	62.8	0.2 ± 6E-3
H₂	0.03	0.02	0.22	0.20	0.41	0.07	0.47	0.001 ± 4E-5

*Rel. Calm 1, Rel. Calm 2 and Rel. Calm 3 correspond to relative calm phases 1, 2 and 3.

volatile concentrations in each eruption phase are representative of the volatile content in the melt, one can observe that the chlorine and carbon dioxide content in the melt decreased over the eruption period, while the fluoride content remained relatively stable. Such fluctuation may reflect the progressive volatile exsolution as the magma ascended to the surface. These volatile concentrations are within the range of magmatic volatiles observed in the context of subduction⁴⁷, with the exception of Cl, which appears relatively enriched, yet supporting the idea of fluid contributions from the subducted slab and associated sediments. The water content (H₂O) varies from 1.01–1.60 wt. % in EDP1, to 1.15–2.13 wt. % in EDP2 and finally 1.19–2.23 wt. % in EDP3. Although a slight increase can be observed over the eruption period, in consistent with a magma ascent, these concentrations are rather low for the subduction zone (Fig. 3), where the global average figure is around 3.9 wt. %⁴⁸. Unfortunately no melt inclusions were analyzed for EDP4 and we assumed that water content was in the range of Phase 3.

Discussion

Eruption triggered by new magma injection

In contrast to the existing data in the literature, the bulk compositions of the samples collected during the eruption onset (EDP1) notably, the large ejected block, display a relatively high silica content (Fig. 4, Supplementary Table 2). The block was stained with sulphur, suggesting regular exposure to a magmatic gas flow. It is thus likely that this block was part of the conduit, which was cleared at eruption onset. The SiO₂ content of this rock was probably increased by the deposition of amorphous or microcrystalline hydrothermal silica in voids and veins⁴⁹. Such void sealing could reduce rock porosity, which in turn promotes pressure build-up during EDP1. The latter unleashed 76 kt of SO₂, an amount surpassing the output of many VEI 3 eruptions such as Shishaldin (63 kt, 1999) or Makian (50 kt, 1988)²⁸, and suggesting the involvement of magmatic processes. The transition from basaltic andesite to a more alkaline basaltic source (Fig. 4, Supplementary Table 2) suggests the arrival of a fresh magma into a relatively evolved melt in the reservoir. Such phenomenon is known to lead to over-pressure (e.g. ref. 50), as new magma disrupts the equilibrium in the reservoir, leading to the exsolution of volatiles, changes in magma composition and viscosity, promoting bubble nucleation, bubble growth, pressure buildup, magma ascent, and a subsequent eruption.

On Ambae, the process was likely accelerated by the rapid heating of the hydrothermal system as magma ascended towards the surface. This led to a swift conversion of subsurface water into steam, triggering volume expansion, which in turn intensified pressure buildup, ultimately resulting in a phreatomagmatic eruption. Similar patterns have been observed during eruptions at other volcanoes^{51–53}.

A basaltic sub-Plinian event

The first papers on the 2017–2018 Ambae eruption did not agree on the strength of the event. They assigned a VEI 3⁵⁴, which means an eruptive column height between 3 and 15 km and a tephra volume of less than 10⁸ m³⁵⁵, to a Plinian eruption²⁰ which suggests a VEI of at least 4 with an eruptive column height that can exceed 25 km and an ejected volume ranging from 0.1 to 10 km³⁵⁶. The volume of the ejected materials is yet to be properly assessed. Alternatively, when looking at the plume heights derived either from the Wellington Volcanic Ash Advisory Centre (VAAC) or from satellite observations⁵⁷ (Fig. 5), it appears that not only did the maximum height of the plume emitted from Ambae vary between 2 and 20 km, but also that it overall increased over the course of the eruptive activity. The maximum height of 20 km was reported on July 28, 2018. This height evolution is consistent with the high SO₂ emissions (Fig. 2; Fig. 5) and emphasizes the increase in eruption intensity from EDP1 to EDP4. Assuming that the plume heights remained at the top of the buoyant column then based on the table compiled in ref. 55, phase 1 (EDP1) was a VEI 2, phase 2 (EDP2) a VEI 3, phase 3 (EDP3) a VEI 4 and phase 4 (EDP4) a VEI 4, with maximum assumed plume heights of 1.5 km, 6.1 km, 18 km, and 20 km respectively (Fig. 5).

Relating the maximum daily values of SO₂ in each eruption phase to the volcanic explosivity index (VEI) according to the following formulation^{28,58}:

$$VEI = [\log_{10}(\text{SO}_2, \text{Tg}) + 3.15] / 0.71 \quad (1)$$

We obtain a VEI 2 for EDP1 and EDP2 with 38 kt and 39 kt respectively (Table 2), while EDP3 with 101 kt may be classified as VEI 3 and EDP4 with 390 kt would be a VEI 4. These two approaches show comparable results and emphasize that the VEI of the eruption can be different depending on the eruption phase. This could explain the divergence of classification in the early works. Overall, based on the above results, Phase 1 may be classified as VEI 2, Phase 2 as VEI 2–3, Phase 3 as VEI 3–4 and Phase 4 as VEI 4. These results confirm what was experienced on the ground, e.g., an eruption of very high intensity, never before experienced or described in the short history of Ambae volcano (Table 1) which increased during the eruption period. The total amount of SO₂ released by the eruption is among the top 5 largest SO₂ contributors through eruption on a global scale²⁸. These observations suggest that Ambae volcano, despite its basaltic magma composition (Fig. 4), is capable of producing at least sub-Plinian VEI 4 events.

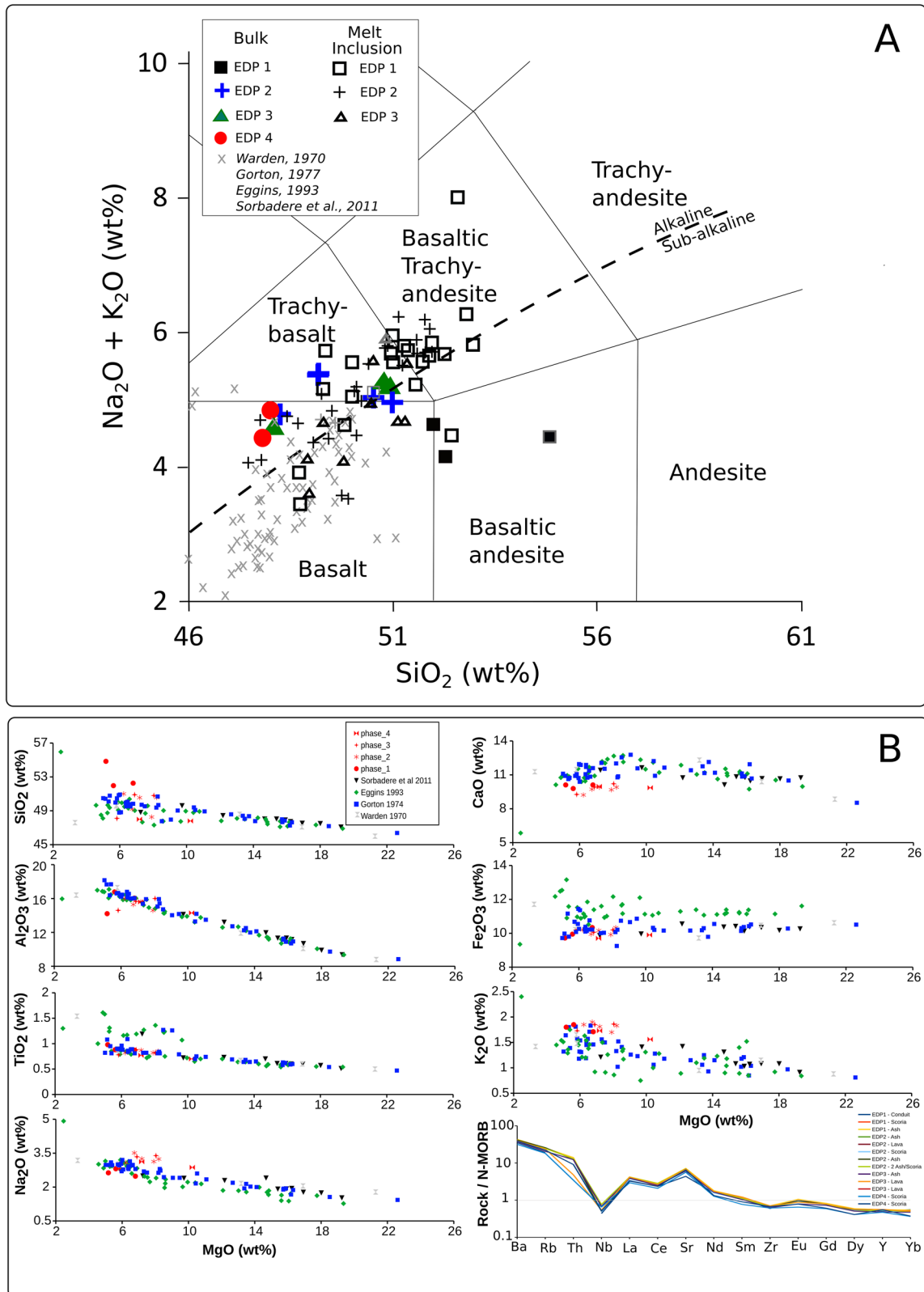


Fig. 4 | Evolution of magma composition throughout the eruption compared to past eruptions. **A** Lava and tephra bulk composition obtained in this work (Supplementary Table 2) are plotted (in red) for comparison with the past results of Warden (1970)⁸⁶, Gordon (1974; 1977)^{87,88}, Eggins (1993)⁸⁹ and Sorbadere et al.⁹⁰. Melt inclusion results (from ref. 20) show a wide range of composition from basaltic trachy-andesite to basalt. The bulk rock and tephra composition from the 2017–2018 show a transition from basaltic andesite and trachy-basalt to basalt compositions. EDP1 corresponds to the onset eruption phase the produces material with relatively high silica content, whilst phase 4 corresponds to the final eruption

phase. Phase 2 and phase 3 correspond to intermediate eruption phases. **B** The Harker diagrams of Ambae samples showing a strong olivine control on the past data⁸⁷ contrasting with a relatively restricted MgO content in this work. The CaO content is lower than the past data, while the K_2O and Na_2O are higher, suggesting a relatively evolved source compared to results from past studies^{86,88–90}. Of the two series defined from the TiO_2 content in the past works⁸⁸, only the low- TiO_2 series is obtained in this work. The trace element concentrations normalized to N-MORB⁹¹ indicate a typical subduction arc source. Results are from bulk rock analyses.

High magma supply rate and volatile-rich source

The amount of magma needed to degas the volume of gas released into the atmosphere during an eruption can be estimated from the ratio of degassed sulfur and the difference between the sulfur in the melt inclusions and in the matrix glass³⁶:

$$M_{\text{magma}} = (M_{\text{Sulfur-gas}} \times 10^6) / (M_{\text{Sulfur-inclusion}} - M_{\text{Sulfur-matrix}}) \quad (2)$$

where M_{magma} is the mass of the magma (in kg) that sustained the eruption, $M_{\text{Sulfur-gas}}$ is the mass of sulfur (in kg) released into the atmosphere, $M_{\text{Sulfur-inclusion}}$ is the amount of sulfur (in ppm) in the melt inclusion and $M_{\text{Sulfur-matrix}}$ is the mass of sulfur (in ppm) in the matrix glass. Assuming that the highest sulfur content in the olivine-pyroxene melt inclusion reflects the undegassed magma source (Supplementary Table 2), and using the above formula, along with the basaltic densities derived from bulk compositions⁵⁹ (Table 4), it is possible to estimate the magma volume required for the eruption. For EDP1, EDP2, EDP3 and EDP4, the required magma volumes are estimated to be 0.014 km³, 0.059 km³, 0.142 km³ and 0.161 km³ respectively (Table 4), totaling 0.376 ± 0.025 km³. Relating these volumes to the duration of each phase yields magma supply rates of 27 m³/s, 17 m³/s, 61 m³/s, and 104 m³/s, respectively. These figures are well above typical rates for basaltic sources, such as those observed at Kilauea (0.6–5.7 m³/s)⁶⁰ or Etna (~0.3 m³/s)⁶¹, the latter remained at constant rate for decades. Ambae's mean magmatic supply rate of 52 m³/s doubles that of nearby Ambrym volcano, where a rate of 25 m³/s was necessary to renew the entire 0.5 km³ magma reservoir within 240 days³¹. This high supply rate likely accounts for Ambrym's status as a top global magmatic degassing source, characterized by continuous intense degassing until 2018^{28,62,63}. As evidenced in instances like La Soufrière⁶⁴, these findings suggest a robust link between magma supply rate and volcanic degassing, implying a direct influence on eruption intensity. The relationship is starkly illustrated during VEI 4 phases (EDP3 and EDP4), sustained by exceptionally high magma supply rate of 61 m³/s and 104 m³/s respectively, coinciding with extreme degassing, each phase releasing 0.9 Mt and 1.1 Mt of SO₂. If we plot for a series of key eruptions³⁶, the associated released SO₂ mass vs. the volume of degassing magma (Eq. 2), the Ambae 2017–2018 stands out for its exceptional gas productivity relative to other basaltic eruptions. This elevated gas/magma proportion (Fig. 6) at Ambae is comparable to that of Ambrym volcano with its 0.5 km³ and a continuous strong degassing^{28,31,63,65} prior to the 2018 eruption. Ambrym has experienced very strong eruptions in the past, including a VEI 4 in 1950 and a probable VEI 6 in 50 A.D.⁶⁶. Ambrym and Ambae share the same geodynamic context and are both influenced by the slightly oblique collision of the buoyant D'Entrecasteaux Ridge (DER)⁶⁷, aided by the influx of a more fertile mantle material with isotopically distinct Indian Ocean-type MORB character^{40,41,68}. The location of Ambrym Volcano well to the south of the southern edge of the D'Entrecasteaux Ridge (DER) may explain the difference in CO₂ levels compared to Ambae volcano. Ambae's location above the carbonate-rich sediments ~650 m-thick transported by the subducted DER may explain its CO₂-enriched magmatic source³⁹. The interaction between DER and the Vanuatu arc began 2–3 million years ago, approximately 100 km to the south of its current position, and migrated northward due to arc curvature and oblique subduction⁶⁹. It is believed that the collision extensively fractured the DER, resulting in deep faults that allow fluids to penetrate and hydrate the oceanic lithospheric mantle⁷⁰. The relatively high thermal parameters of the Australian plate at depth, enables hydrated minerals to reach deeply into the mantle before dehydrating⁷⁰. These processes may play a crucial role in the formation of volatile-rich, deep magma sources, that may subsequently trigger large-scale basaltic explosive eruptions, as demonstrated by the activity on Ambae. Recognizing the fundamental role of volatiles in regulating magma ascent from depth, it is reasonable to assume that they contributed to the rapid magma ascent observed on Ambae²⁰. These results therefore suggest that rapid magma ascent towards the surface required to produce basaltic Plinian eruptions⁷¹ reflected a

magmatic sources richly saturated in volatiles. With a high volatile content, the magmatic mixture becomes more buoyant due to an increased volume fraction of exsolved gas, thereby expediting magma ascent.

The role of degassing in the transition from effusive to explosive activity

The analysis of the interplay between VRP variations and SO₂ emissions throughout the eruptive period unfolds a consistent pattern, delineated into five distinct episodes (Fig. 5). Indeed, excluding the phreatomagmatic onset phase (Phase 1), the subsequent three eruptive phases can be divided into the following 5 episodes (Fig. 5): a period of relative calm following a vigorous eruptive phase (here after as EPS1 or Eruption Phase Sequence 1), followed by a phase characterized by magma emergence at the surface (EPS2), featuring lava fountains, lava flows, and strombolian activity (lava flows being restricted to eruption phase 2). The 3rd episode is characterized by sustained lava fountaining (EPS3), leading to a sudden gas surge that triggered explosive manifestations (EPS4), and finally a phase marked by persistent of gas surges whilst the top of magma column receded to depth (EPS5). This pattern illustrates the transition from effusive to explosive character, underscoring that the primary controlling factor is gas. Each eruptive phase commenced with an effusive type manifestation that progressed into explosive as gas increased. A general trend can also be discerned for the eruption as a whole, in which the amount of gas released during the explosive phases increased from EDP2 (0.5 Tg SO₂), being more effusive nature, to EDP3 (0.9 Tg SO₂) and then EDP4 (1.1 Tg SO₂). This increase further emphasizes that the intensity of eruptive activity is driven by the amount of available volatiles, which facilitate a high rate of magma supply and an extremely fast ascent speed (15–270 km/h)²⁰. This rapid ascent led to substantial undercooling and subsequent rapid crystallization⁷², a process known to increase magma viscosity, which is a critical precursor to fragmentation. The rapid magma ascent from the shallow reservoir (0.5–3 km)²⁰, posed a challenge for effectively decoupling of volatiles from the melt. This is another crucial process for highly explosive eruptions in basaltic volcanoes^{67,71}, as seen in phase 3 and phase 4. The likelihood of producing basaltic explosive events increases with a lower H₂O content, as observed on Ambae, with 1–2 wt. % of H₂O (Fig. 3; Supplementary Table 2), compared to the 2–6 wt. % typically observed in basaltic arc magmas⁴⁷. Recent studies indicate that low H₂O content increases magma viscosity in the conduit and that even small amounts of external water can induce a shift from explosive to lava fountain eruption styles⁷¹.

While many studies have implicated high levels of CO₂ in magma as responsible for more explosive eruptions^{8,73–75}, this topic remains controversial. At Ambae, the decrease in CO₂ concentrations in melt inclusions, dropping from 3900 ppm to 900 ppm, amid an escalation eruption intensity (Supplementary Table 2) does not support this idea. However, this decrease can be attributed to the exsolution of CO₂, a process that not only enhances magma buoyancy, facilitating its ascent, but it may also increase the amount of volatiles present adding more pressure in the reservoir and conduit.

Conclusion

The 2017–2018 Ambae eruption stands out as a unique case in which the total gas emissions of a basaltic sub-Plinian event have been quantified in parallel with thermal heat fluxes. The data show very high levels of degassing with a total eruptive release of 130 Tg H₂O, 6.8 Tg CO₂, 3.3 Tg SO₂, 0.2 Tg H₂S and 0.001 Tg H₂. The total SO₂ output ranks Ambae at 6th position on the list of eruptions with quantified SO₂ output. The total CO₂ release was substantial for a single volcano, equivalent to the annual CO₂ output from of all Latin American volcanoes. Surprisingly, the magma volume sustaining this enormous gas output is modest compared to other basaltic volcanoes, implying a volatile-rich magma source beneath Ambae. We propose the volatile-rich nature of Ambae magma is probably linked to the regional geodynamic environment. Indeed, the subduction of the extensively fractured D'Entrecasteaux Ridge, with its carbonate-rich sediments, associated to the high thermal gradient and

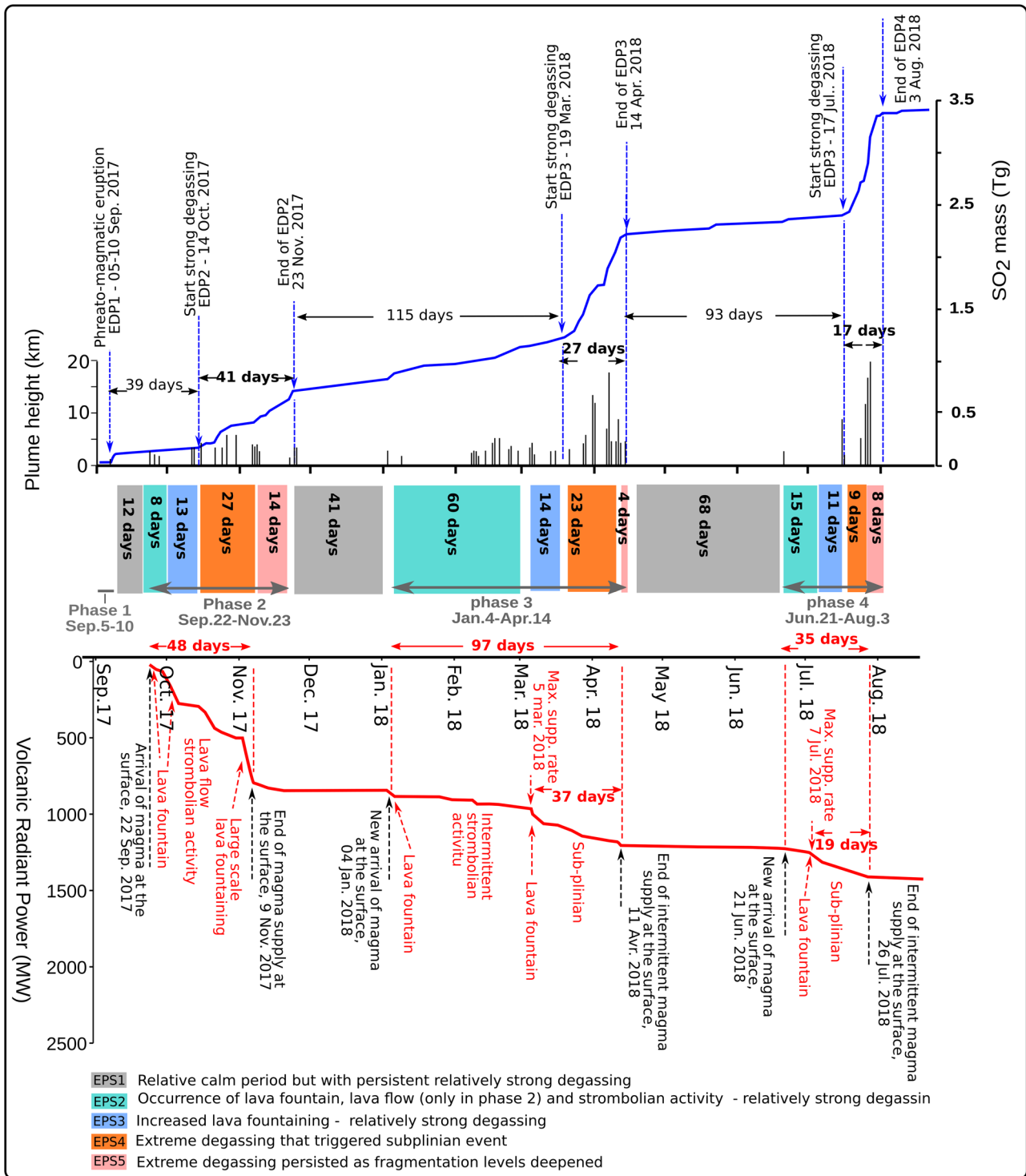


Fig. 5 | VRP and SO₂ mass reveal a distinct pattern repeated across the four intense eruption phases. The juxtaposition of the cumulative values of volcanic radiative power (VRP) and sulfur dioxide (SO₂) mass reveals a discernible pattern that can be divided into 5 distinct episodes that characterize each of the three eruption phases. It also underlines the time lag between the appearance of hot magmatic features at the surface and the SO₂ surges. Lava fountain episodes are

characterized by a rapid rise in VRP, which typically precedes the intense explosive activity. Plume heights derived from data provided by the Volcanic Ash Advisory Center (VAAC), satellite imagery, and on-site observations, collectively indicate an increase of the eruption duration, corresponding to an escalation in eruptive intensity.

the westward uprising fertile mantle likely favor the formation of a volatile-rich magma. A high content of dissolved volatiles can lead to extensive exsolution, which increases magma buoyancy and may result in a higher magma supply and faster ascent. The rapid ascent of the magma creates challenges in separating volatiles from the melt,

which favor magma into a highly explosive basaltic eruptions. The results also highlight the role of gas surges in the transition from effusive to explosive volcanic activity. Without a substantial influx of volatiles, the 2017–2018 eruption at Ambae would likely have been predominantly effusive.

Table 4 | The volume of magma that sustained 2017–2018 eruption of Ambae

	Erupt. phase 1 September 5–10 (6 days)	Rel. Calm 1 September 11–October 13 (33 days)	Erupt. phase 2 October 14–November 23 (41 days)	Rel.calm 2 November 24–March 18 (115 days)	Erupt. phase 3 March 19–April 14 (27 days)	Rel. Calm 3 April 15–July 16 (93 days)	Erupt. phase 4 July 17– August 03 (18 days)
Total amount of S released (kt)	38	29	258	235	472	89	537
Max S value in MI (ppm)	980	980	1541	1541	1183	1183	1183
Mean S in matrix (ppm)	361	361	509	509	353	353	353
Density (kg/m ³)	2802	2802	2823	2823	2821	2821	2819
Deg.magma Mass (Mt)	38.8	29.2	167.5	152.5	399.3	75.0	397.9
Volume (km ³)	0.014 (63.2%)	0.010 (63.2%)	0.059 (67.0%)	0.054 (67.0%)	0.142 (70.2%)	0.027 (70.2%)	0.161 (70.2%)
Magma suppl. Rate (m ³ /s)	26.7	3.7	16.8	5.4	60.7	3.3	103.6

Mean magmatic supply rate during strong eruption phases: 52 m³/s.
 Cumulative degassed magma during eruptive phases 1, 2, 3 and 4 (km³): 0.376 ± 0.025.
 Cumulative degassed magma during relative calm phases 1, 2 and 3 (km³): 0.091 ± 0.002.
 Total degassed magma volume: 0.467 ± 0.027 km³.

Methods

SO₂ mass from Satellite sensors

The quantity of SO₂ released during the Ambae 2017–2018 eruption was estimated using daily SO₂ mass captured above the Ambae volcano by the Ozone Mapping and Profiler Suite (OMPS) and the Ozone Monitoring Instrument (OMI). The data series, available online at <https://so2.gsfc.nasa.gov/>, were compiled and analyzed for the entire eruptive period, from September 5, 2017, to August 3, 2018. The most intense SO₂ output of July 28, 2018 was followed thanks to TROPOMI measurements. The nearby Ambrym volcano also contributed to the daily SO₂ mass, but its contribution was estimated and then excluded from the total SO₂ mass, especially during relative calm phases, based on the area covered and the corresponding DU according to the method in ref. 51 During the four extreme degassing phases, Ambrym’s output was negligible and therefore ignored in the daily values. Yasur volcano, located in the south of Vanuatu, had a negligible impact throughout the eruption period. In contrast there was a notable SO₂ output from the Tinakula eruption on October 21, 2017, but that contribution was also excluded in the compilation.

Airborne and scanning DOAS measurements

In the early eruption phase, two DOAS campaigns were carried out, on October 3 and October 6, 2017, using airborne traverses and stationary scanning measurements. Airborne traverses were performed following the approach outlined in ref. 21 using a Brittan-Norman Islander flying beneath the plume at 8–12 km from the source whilst scanning DOAS were carried out beneath the plume on the western part of Ambae at the about 14 km from the source using the same approach outlined in ref. 76 Due to the increasing activity and the effective cost of the campaigns, no further measurements were carried out.

Volcanic Radiant Power (VRP) and Time Average Discharge Rate (TADR)

The variation of thermal radiation emitted during the eruption period by hot surfaces at the summit of Ambae volcano was recorded by the Moderate Resolution Imaging Spectroradiometer (MODIS). These data were made available to the scientific community and observatories through MODVOLC (MODIS Volcanic Activity Monitoring), MIROVA (Middle Infra-Red Observation of Volcanic Activity) and Mounts (Mounts Project). In this work, the thermal dynamics of the eruptive activity are based primarily on data from MIROVA who provided VRPs in near real time⁷⁷. Specifically, the VRP is calculated as follows:

$$VRP = 18.9 A_{\text{pixel}} \sum_1^{\text{npix}} (L_{\text{MIR,alert}} - L_{\text{MIR,bk}})_i \tag{3}$$

where npix is the number of alerted pixels, $L_{\text{MIR,alert}}$ is the pixel integrated MIR radiance of the *i*th alerted pixel, $L_{\text{MIR,bk}}$ is the MIR radiance of the background (average radiance of pixels surrounding the anomaly), A_{pixel} is the pixel size (1 km² for the resampled MODIS pixels), and 18.9 is a constant of proportionality⁷⁷

The VRP (in W) is then convert into TADR (m³/s) according to the following equation⁴⁴:

$$TADR = VRP/C_{\text{rad}} \tag{4}$$

where C_{rad} is the radiant density expressed in J/m³ and can be predicted on the basis of the silica content of the erupted products:

$$C_{\text{rad}} = 6.45 \times 10^{25} \times (X_{\text{SiO}_2})^{-10.4} \tag{5}$$

where X_{SiO_2} is the silica content (wt. %) of the erupted magma. The cumulated TADR over the eruption period has allowed broad estimation of extruded magma volume.

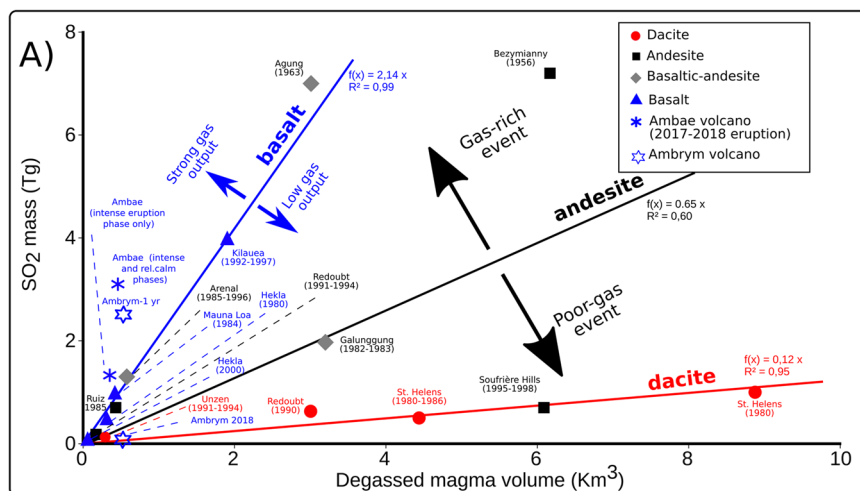


Fig. 6 | Relationship between SO₂ mass and magma volume across different magma types, emphasizing basaltic gas-rich events. A Relationship between SO₂ mass and the corresponding magma volume sustaining past eruptive events. It distinguishes the magnitude of gas output during eruptive events as a function of magma type. The blue, black and red lines are regression lines between SO₂ releases during eruptions and corresponding magma source volumes for basalt, andesite and dacite respectively. The dashed lines are included to clearly distinguish the individual eruptions for better visualization. Bezymianny (1956) and Nevado del Ruiz (1985) eruptions were gas-rich events, whilst Soufrière Hills eruption (1995–1998)

was a gas-poor event for andesitic magma. Agung (1963) and Arenal (1985–1996) eruptions are gas-rich events contrasting with Galunggung (1982–1983) for basaltic-andesite magma. Similarly, in the case of basaltic magma, Ambae 2017–2018 eruption stands out as a gas-rich event. The relatively calm phases contributed significantly to the overall release of SO₂. Ambrym's situation in 2005–2015 shares this same analysis with its annual 2.5 Tg of SO₂⁶² while the 2018 eruption was gas-poor event suggesting a degassed source. Dacite magmas are poor-gas source. Data are recalculated from ref. 36.

Gas composition

The gas composition of Ambae was measured using a Multicomponent Gas Analyser System (Multi-GAS)^{78,79}. This portable instrument measures the concentrations of CO₂, SO₂, H₂S, H₂, as well as ambient atmospheric pressure (P), temperature (T), and relative humidity (RH). This latter is converted into plume H₂O concentration following the approach outlined in ref. 80:

$$H_2O = 6.1121 * (1.0007 + 3.46P^{-6}) * \exp((17.502 * T)/(240.97 + T)) * (Rh/100 * 10^6) \quad (6)$$

where H₂O is the water vapor content in ppmv, P is the pressure in mbar, T is the air temperature in °C, and Rh is the relative humidity in %. The CO₂ is measured with a commercial infrared spectrometer (range 0–3000 ppm) whereas SO₂, H₂S, H₂ gases were quantified using specific electrochemical sensors (typical range 0–200 ppm). On May 22, 2018, the MultiGAS was first positioned on Voui crater rim, but given the distance to the active vent and the dynamic of the degassing, the plume never reached the device. The decision was then taken to move the system to the rim of the new cone in the Voui's crater. The system was placed in the plume, however given the relatively dangerous exposure to the activity, only about a quarter of an hour has been successfully devoted to this gas recording.

Field sampling and Laboratory analyses

Three field campaigns at the summit of the Ambae volcano were carried out on October 16, 2017, January 6, 2018 and May 21–22, 2018. During these expeditions ash, scoria and rock samples were collected for laboratory analyses. Complementary sampling were carried out on the western part of Ambae island by local inhabitants, immediately after ash falls. Samples collected were analyzed for major elements using ICP-AES, after dissolution of 100 mg of finely crushed sample by alkaline fusion. Trace-element concentrations were measured by ICP-MS after the dissolution of 100 mg of each sample, following the approach outlined in ref. 81 Comparison with repeated analysis of international standards (AVG-2, BIR-1, and BEN) was used to validate major and trace element data. For the major elements, the precision is better than 5%, whilst the precision is less than 10% for all the trace elements. Analyses were carried out in Laboratoire Magma et Volcans

(Clermont-Ferrand, France) and Laboratoire Géosciences Océans (Brest, France).

Volatile (H₂O, CO₂, Cl, F, S) content in melt inclusions and matrix glasses is sourced from ref. 20 which provides a detailed description of the methodology, including post entrapment crystallization and modeling.

Data availability

The data required to produce all figures are available in this manuscript and in ref. 20 for melt inclusions data.

Received: 3 July 2024; Accepted: 9 January 2025;

Published online: 04 February 2025

References

- Blackburn, E. A., Wilson, L. & Sparks, R. S. J. Mechanisms and dynamics of strombolian activity. *J. Geol. Soc.* **132**, 429–440 (1976).
- Wilson, L. & Head, J. W. III Ascent and eruption of basaltic magma on the Earth and Moon. *J. Geophys. Res. Solid Earth* **86**, 2971–3001 (1981).
- Vergnolle, S. & Jaupart, C. Separated two-phase flow and basaltic eruptions. *J. Geophys. Res. Solid Earth* **91**, 12842–12860 (1986).
- Sable, J. E., Houghton, B. F., Del Carlo, P. & Coltelli, M. Changing conditions of magma ascent and fragmentation during the Etna 122 BC basaltic Plinian eruption: Evidence from clast microtextures. *J. Volcanol. Geotherm. Res.* **158**, 333–354 (2006).
- Parfitt, E. A. & Wilson, L. Explosive volcanic eruptions—IX. The transition between Hawaiian-style lava fountaining and Strombolian explosive activity. *Geophys. J. Int.* **121**, 226–232 (1995).
- Bamber, E. C. et al. Outgassing behaviour during highly explosive basaltic eruptions. *Commun. Earth Environ.* **5**, 1–16 (2024).
- Jordan, S. C., Le Penec, J.-L., Gurioli, L., Roche, O. & Boivin, P. Highly explosive eruption of the monogenetic 8.6 ka BP La Vache et Lassolas scoria cone complex (Chaîne des Puys, France). *J. Volcanol. Geotherm. Res.* **313**, 15–28 (2016).
- Allison, C. M., Roggensack, K. & Clarke, A. B. Highly explosive basaltic eruptions driven by CO₂ exsolution. *Nat. Commun.* **12**, 217 (2021).

9. Newhall, C. G. & Self, S. The volcanic explosivity index (VEI) an estimate of explosive magnitude for historical volcanism. *J. Geophys. Res. Oceans* **87**, 1231–1238 (1982).
10. Stelling, P. et al. Geology and petrology of ejecta from the 1999 eruption of Shishaldin Volcano, Alaska. *Bull. Volcanol.* **64**, 548–561 (2002).
11. Caplan-Auerbach, J. & McNutt, S. R. New insights into the 1999 eruption of Shishaldin volcano, Alaska, based on acoustic data. *Bull. Volcanol.* **65**, 405–417 (2003).
12. Williams, S. N. *Geology and Eruptive Mechanisms of Masaya Caldera Complex, Nicaragua*. (Dartmouth College, 1983).
13. Walker, J. A., Williams, S. N., Kalamarides, R. I. & Feigenson, M. D. Shallow open-system evolution of basaltic magma beneath a subduction zone volcano: The Masaya Caldera Complex, Nicaragua. *J. Volcanol. Geotherm. Res.* **56**, 379–400 (1993).
14. Pérez, W. & Freundt, A. The youngest highly explosive basaltic eruptions from Masaya Caldera (Nicaragua): Stratigraphy and hazard assessment. in *Volcanic Hazards in Central America* (eds. Rose, W. I. et al) vol. 412 0 (Geological Society of America, 2006).
15. Costantini, L., Bonadonna, C., Houghton, B. F. & Wehrmann, H. New physical characterization of the Fontana Lapilli basaltic Plinian eruption, Nicaragua. *Bull. Volcanol.* **71**, 337–355 (2009).
16. Zurek, J., Moune, S., Williams-Jones, G., Vigouroux, N. & Gauthier, P.-J. Melt inclusion evidence for long term steady-state volcanism at Las Sierras-Masaya volcano, Nicaragua. *J. Volcanol. Geotherm. Res.* **378**, 16–28 (2019).
17. Coltelli, M., Del Carlo, P. & Vezzoli, L. Discovery of a Plinian basaltic eruption of Roman age at Etna volcano, Italy. *Geology* **26**, 1095–1098 (1998).
18. Houghton, B. F. et al. The influence of conduit processes on changes in style of basaltic Plinian eruptions: Tarawera 1886 and Etna 122 BC. *J. Volcanol. Geotherm. Res.* **137**, 1–14 (2004).
19. Schaubroth, J. et al. Conduit margin heating and deformation during the AD 1886 basaltic Plinian eruption at Tarawera volcano, New Zealand. *Bull. Volcanol.* **78**, 12 (2016).
20. Moussallam, Y. et al. Fast ascent rate during the 2017–2018 Plinian eruption of Ambae (Aoba) volcano: a petrological investigation. *Contrib. Mineral. Petrol.* **174**, 90 (2019).
21. Bani, P. et al. Remarkable geochemical changes and degassing at Vouli crater lake, Ambae volcano, Vanuatu. *J. Volcanol. Geotherm. Res.* **188**, 347–357 (2009).
22. Wiart, P. *Impact et gestion des risques volcaniques au Vanuatu: document de travail*. <https://www.documentation.ird.fr/hor/fdi:43111> (1995).
23. Bani, P. et al. Characteristics of the summit lakes of Ambae volcano and their potential for generating lahars. *Nat. Hazards Earth Syst. Sci.* **9**, 1471–1478 (2009).
24. Németh, K., Cronin, S. J., Charley, D., Harrison, M. & Garae, E. Exploding lakes in Vanuatu — “Surtseyan-style” eruptions witnessed on Ambae Island. *Episodes J. Int. Geosci* **29**, 87–92 (2006).
25. Coppola, D., Laiolo, M. & Cigolini, C. Fifteen years of thermal activity at Vanuatu’s volcanoes (2000–2015) revealed by MIROVA. *J. Volcanol. Geotherm. Res.* **322**, 6–19 (2016).
26. Haruel, C., Bani, P., Tari, D., Nauret, F., & Rose-Koga, E. Formation of new beaches from lahar deposits, Ambae volcano, Vanuatu. *Bulletin of Volcanology* (Under Review).
27. Kloss, C. et al. Impact of the 2018 Ambae eruption on the global stratospheric aerosol layer and climate. *J. Geophys. Res. Atmospheres* **125**, e2020JD032410 (2020).
28. Carn, S. A., Clarisse, L. & Prata, A. J. Multi-decadal satellite measurements of global volcanic degassing. *J. Volcanol. Geotherm. Res.* **311**, 99–134 (2016).
29. Fischer, T. P. et al. The emissions of CO₂ and other volatiles from the world’s subaerial volcanoes. *Sci. Rep.* **9**, 18716 (2019).
30. Aiuppa, A., Fischer, T. P., Plank, T. & Bani, P. CO₂ flux emissions from the Earth’s most actively degassing volcanoes, 2005–2015. *Sci. Rep.* **9**, 5442 (2019).
31. Allard, P. et al. Prodigious emission rates and magma degassing budget of major, trace and radioactive volatile species from Ambrym basaltic volcano, Vanuatu island Arc. *J. Volcanol. Geotherm. Res.* **322**, 119–143 (2016).
32. Métrich, N. et al. Magma and volatile supply to post-collapse volcanism and block resurgence in Siwi Caldera (Tanna Island, Vanuatu Arc). *J. Petrol* **52**, 1077–1105 (2011).
33. Lages, J. et al. First in-situ measurements of plume chemistry at Mount Garet Volcano, Island of Gaua (Vanuatu). *Appl. Sci.* **10**, 7293 (2020).
34. Gertisser, R. & Keller, J. Trace Element and Sr, Nd, Pb and O Isotope Variations in Medium-K and High-K Volcanic Rocks from Merapi Volcano, Central Java, Indonesia: Evidence for the Involvement of Subducted Sediments in Sunda Arc Magma Genesis. *J. Petrol.* **44**, 457–489 (2003).
35. Alfianti, H. et al. Bromo activity over the last decade: consistent passive degassing and source magma evolution. *Geosci. Lett.* **9**, 15 (2022).
36. Shinohara, H. Excess degassing from volcanoes and its role on eruptive and intrusive activity. *Rev. Geophys.* **46**, (2008).
37. Aiuppa, A., Fischer, T. P., Plank, T., Robidoux, P. & Di Napoli, R. Along-arc, inter-arc and arc-to-arc variations in volcanic gas CO₂/ST ratios reveal dual source of carbon in arc volcanism. *Earth-Sci. Rev.* **168**, 24–47 (2017).
38. Plank, T. & Langmuir, C. H. The chemical composition of subducting sediment and its consequences for the crust and mantle. *Chem. Geol.* **145**, 325–394 (1998).
39. Collot, J.-Y. et al. Geology of the d’Entrecasteaux-New Hebrides arc collision zone: results from a deep submersible survey. *Tectonophysics* **212**, 213–241 (1992).
40. Monzier, M., Robin, C., Eissen, J.-P. & Cotten, J. Geochemistry vs. seismo-tectonics along the volcanic New Hebrides Central Chain (Southwest Pacific). *J. Volcanol. Geotherm. Res.* **78**, 1–29 (1997).
41. Briquieu, L. et al. Sr, Nd and Pb isotopic composition of volcanic and volcanoclastic samples of ODP Leg 134. *Supplement to: Briquieu, L et al. (1994): Temporal magmatic evolution of the Aoba Basin, Central New Hebrides Island Arc: Pb, Sr, and Nd isotopic evidence for the coexistence of two mantle components beneath the Arc*. In: Green, HG; Collot, J.-Y; Stokking, LB; et al. (eds.), Proceedings of the Ocean Drilling Program, Scientific Results, College Station, TX (Ocean Drilling Program), 134, 393–401, 10.2973/odp.proc.sr.134.019.1994 PANGAEA <https://doi.org/10.1594/PANGAEA.787578> (1994).
42. Wright, R., Flynn, L., Garbeil, H., Harris, A. & Pilger, E. Automated volcanic eruption detection using MODIS. *Remote Sens. Environ.* **82**, 135–155 (2002).
43. Coppola, D., Laiolo, M., Cigolini, C., Donne, D. D. & Ripepe, M. Enhanced volcanic hot-spot detection using MODIS IR data: results from the MIROVA system. *Geol. Soc. Lond. Spec. Publ.* **426**, 181–205 (2016).
44. Coppola, D., Piscopo, D., Staudacher, T. & Cigolini, C. Lava discharge rate and effusive pattern at Piton de la Fournaise from MODIS data. *J. Volcanol. Geotherm. Res.* **184**, 174–192 (2009).
45. Ikeda, Y. et al. Contributions of slab fluid and sediment melt components to magmatism in the Mariana Arc–Trough system: Evidence from geochemical compositions and Sr, Nd, and noble gas isotope systematics. *Isl. Arc* **25**, 253–273 (2016).
46. Cannatelli, C., Doherty, A. L., Esposito, R., Lima, A. & De Vivo, B. Understanding a volcano through a droplet: A melt inclusion approach. *J. Geochem. Explor.* **171**, 4–19 (2016).
47. Wallace, P. J. Magmatic Volatiles. in *Encyclopedia of Geology (Second Edition)* (eds. Alderton, D. & Elias, S. A.) 301–312 <https://doi.org/10.1038/s43247-025-02018-5>

- [org/10.1016/B978-0-08-102908-4.00097-7](https://doi.org/10.1016/B978-0-08-102908-4.00097-7) (Academic Press, Oxford, 2021).
48. Plank, T., Kelley, K. A., Zimmer, M. M., Hauri, E. H. & Wallace, P. J. Why do mafic arc magmas contain ~4wt% water on average? *Earth Planet. Sci. Lett.* **364**, 168–179 (2013).
 49. Boudon, G., Villemant, B., Komorowski, J.-C., Ildefonse, P. & Semet, M. P. The hydrothermal system at Soufriere Hills Volcano, Montserrat (West Indies): Characterization and role in the on-going eruption. *Geophys. Res. Lett.* **25**, 3693–3696 (1998).
 50. Woods, A. W. & Cowan, A. Magma mixing triggered during volcanic eruptions. *Earth Planet. Sci. Lett.* **288**, 132–137 (2009).
 51. Bani, P. et al. The 2009–2010 eruption of Gaua volcano (Vanuatu archipelago): Eruptive dynamics and unsuspected strong halogens source. *J. Volcanol. Geotherm. Res.* **322**, 63–75 (2016).
 52. Primulyana, S., Bani, P. & Harris, A. The effusive-explosive transitions at Rokatenda 2012–2013: unloading by extrusion of degassed magma with lateral gas flow. *Bull. Volcanol.* **79**, 22 (2017).
 53. Bani, P., Kristianto, Kunrat, S. & Syahbana, D. K. Insights into the recurrent energetic eruptions that drive Awu, among the deadliest volcanoes on Earth. *Nat. Hazards Earth Syst. Sci.* **20**, 2119–2132 (2020).
 54. Knepp, T. N. et al. Identification of smoke and sulfuric acid aerosol in SAGE III/ISS extinction spectra. *Atmospheric Meas. Tech.* **15**, 5235–5260 (2022).
 55. Pyle, D. M. Chapter 13 - Sizes of Volcanic Eruptions. in *The Encyclopedia of Volcanoes (Second Edition)* (ed. Sigurdsson, H.) 257–264 <https://doi.org/10.1016/B978-0-12-385938-9.00013-4> (Academic Press, Amsterdam, 2015).
 56. Cioni, R., Pistolesi, M. & Rosi, M. Chapter 29 - Plinian and Subplinian Eruptions. in *The Encyclopedia of Volcanoes (Second Edition)* (ed. Sigurdsson, H.) 519–535 <https://doi.org/10.1016/B978-0-12-385938-9.00029-8> (Academic Press, Amsterdam, 2015).
 57. Malinina, E. et al. Changes in stratospheric aerosol extinction coefficient after the 2018 Ambae eruption as seen by OMPS-LP and MAECHAM5-HAM. *Atmospheric Chem. Phys.* **21**, 14871–14891 (2021).
 58. Bani, P. et al. Modest volcanic SO₂ emissions from the Indonesian archipelago. *Nat. Commun.* **13**, 3366 (2022).
 59. Lange, R. L. & Carmichael, I. S. E. Thermodynamic properties of silicate liquids with emphasis on density, thermal expansion and compressibility. *Rev. Mineral. Geochem.* **24**, 25–64 (1990).
 60. Dvorak, J. J. & Dzirisin, D. Variations in magma supply rate at Kilauea Volcano, Hawaii. *J. Geophys. Res. Solid Earth* **98**, 22255–22268 (1993).
 61. Palano, M., Pezzo, G. & Chiarabba, C. Magma budget, plutonic growth and lateral spreading at Mt. Etna. *Commun. Earth Environ.* **5**, 1–9 (2024).
 62. Carn, S. A., Fioletov, V. E., McLinden, C. A., Li, C. & Krotkov, N. A. A decade of global volcanic SO₂ emissions measured from space. *Sci. Rep.* **7**, 44095 (2017).
 63. Bani, P. et al. First estimate of volcanic SO₂ budget for Vanuatu island arc. *J. Volcanol. Geotherm. Res.* **211–212**, 36–46 (2012).
 64. Sparks, S. R. J. et al. Analysis of magma flux and eruption intensity during the 2021 explosive activity at La Soufrière, St Vincent, West Indies. *Geol. Soc. Lond. Spec. Publ.* **539**, 63–79 (2024).
 65. Bani, P. et al. Surge in sulphur and halogen degassing from Ambrym volcano, Vanuatu. *Bull. Volcanol.* **71**, 1159–1168 (2009).
 66. Global Volcanism Program, Smithsonian Institution & Venzke, E. *Volcanoes of the World*, v. 4.3.4. Global Volcanism Program (2013).
 67. Deng, C., Jenner, F. E., Wan, B. & Li, J.-L. The influence of ridge subduction on the geochemistry of Vanuatu Arc Magmas. *J. Geophys. Res. Solid Earth* **127**, e2021JB022833 (2022).
 68. Peate, D. W. et al. Geochemical variations in vanuatu arc lavas: the role of subducted material and a variable mantle wedge composition. *J. Petrol.* **38**, 1331–1358 (1997).
 69. Greene, H. & Collot, J.-Y. Ridge-Arc Collision: Timing and Deformation Determined by Leg 134 Drilling, Central New Hebrides Island Arc. *Proc Ocean Drill Program Sci Results* **134**, (1994).
 70. Baillard, C., Crawford, W. C., Ballu, V., Pelletier, B. & Garaebiti, E. Tracking subducted ridges through intermediate-depth seismicity in the Vanuatu subduction zone. *Geology* **46**, 767–770 (2018).
 71. La Spina, G., Arzilli, F., Burton, M. R., Polacchi, M. & Clarke, A. B. Role of volatiles in highly explosive basaltic eruptions. *Commun. Earth Environ.* **3**, 1–13 (2022).
 72. Arzilli, F. et al. Magma fragmentation in highly explosive basaltic eruptions induced by rapid crystallization. *Nat. Geosci.* **12**, 1023–1028 (2019).
 73. Allard, P. A CO₂-rich gas trigger of explosive paroxysms at Stromboli basaltic volcano, Italy. *J. Volcanol. Geotherm. Res.* **189**, 363–374 (2010).
 74. Aiuppa, A. et al. First observational evidence for the CO₂-driven origin of Stromboli's major explosions. *Solid Earth* **2**, 135–142 (2011).
 75. Helo, C., Longpré, M.-A., Shimizu, N., Clague, D. A. & Stix, J. Explosive eruptions at mid-ocean ridges driven by CO₂-rich magmas. *Nat. Geosci.* **4**, 260–263 (2011).
 76. Bani, P. et al. Dukono, the predominant source of volcanic degassing in Indonesia, sustained by a depleted Indian-MORB. *Bull. Volcanol.* **80**, 5 (2017).
 77. Coppola, D. et al. Thermal Remote Sensing for Global Volcano Monitoring: Experiences From the MIROVA System. *Front. Earth Sci.* **7**, (2020).
 78. Aiuppa, A., Federico, C., Giudice, G. & Gurrieri, S. Chemical mapping of a fumarolic field: La Fossa Crater, Vulcano Island (Aeolian Islands, Italy). *Geophys. Res. Lett.* **32**, (2005).
 79. Shinohara, H. A new technique to estimate volcanic gas composition: plume measurements with a portable multi-sensor system. *J. Volcanol. Geotherm. Res.* **143**, 319–333 (2005).
 80. Buck, A. L. New equations for computing vapor pressure and enhancement factor. *J. Appl. Meteorol. Climatol.* **20**, 1527–1532 (1981).
 81. Barrat, J. A. et al. Determination of rare earth elements in sixteen silicate reference samples by Icp-MS after Tm addition and ion exchange separation. *Geostand. News/* **20**, 133–139 (1996).
 82. Philipson Bani (IRD/LMV) [@philipsonbani]. Night fall in the middle of the day - Ambae eruption <https://t.co/HO6yoJKbkK>. Twitter <https://x.com/philipsonbani/status/1022480655110864897> (2018).
 83. Stix, J. & de Moor, J. M. Understanding and forecasting phreatic eruptions driven by magmatic degassing. *Earth Planets Space* **70**, 83 (2018).
 84. Bani, P. et al. Heterogeneity of volatile sources along the Halmahera arc, Indonesia. *J. Volcanol. Geotherm. Res.* **418**, 107342 (2021).
 85. Wallace, P. J. Volatiles in subduction zone magmas: concentrations and fluxes based on melt inclusion and volcanic gas data. *J. Volcanol. Geotherm. Res.* **140**, 217–240 (2005).
 86. Warden, A. J. Evolution of Aoba caldera volcano, New Hebrides. *Bull. Volcanol.* **34**, 107–140 (1970).
 87. Gorton, M. P. The geochemistry and origin of quaternary volcanism in the New Hebrides. *Geochim. Cosmochim. Acta* **41**, 1257–1270 (1977).
 88. Gorton, M. P. *The Geochemistry and Geochronology of the New Hebrides*. (The Australian National University (Australia), 1974).
 89. Eggins, S. M. Origin and differentiation of picritic arc magmas, Ambae (Aoba), Vanuatu. *Contrib. Mineral. Petrol.* **114**, 79–100 (1993).
 90. Sorbadere, F., Schiano, P., Metrich, N. & Garaebiti, E. Insights into the origin of primitive silica-undersaturated arc magmas of Aoba volcano (Vanuatu arc). *Contrib. Mineral. Petrol.* **162**, 995–1009 (2011).
 91. Hofmann, A. W. Chemical differentiation of the Earth: the relationship between mantle, continental crust, and oceanic crust. *Earth Planet. Sci. Lett.* **90**, 297–314 (1988).

Acknowledgements

This work was supported by the IRD (Institute of Research for Development) in collaboration with the VMGD (Vanuatu Meteorology and Geohazards Department) and the residents of Ambae Island. Field assessment and samplings were funded by IRD and VOLVAN program with additional support from EMVOLDIVA. We extend our gratitude to Mhammed Benbakkar (LMV) and Céline Liorzou (Geo-Ocean) for the ICP-AES analyses. The manuscript greatly benefits from constructive feedback provided by Carolina Ortiz Guerrero and the anonymous reviewer. This is Laboratory of Excellence Clervolc contribution n° 680.

Author contributions

P. Bani led the conceptualization of the research, field sampling and measurements, data analysis and interpretation, as well as the writing and revision of the paper. D. Tari and I. Bani participated in the rare field sampling conducted during the eruption period and contributed to the interpretation of the data. Satellite data were analyzed by D. Coppola for thermal radiation and by S. Carn for SO₂ emissions. They both contributed to the writing of the manuscript. A. Aiuppa analyzed the geochemical gas data and provided comprehensive interpretations of the results. D. Cluzel provided a thorough interpretation of the data within the geodynamic context. E. Rose-Koga and Y. Moussallam conducted the laboratory analyses of melt inclusions, while F. Nauret and E. Médard performed the geochemical and petrological analyses. All contributed to the writing of the manuscript.

Competing interests

The authors declare no competing interests

Additional information

Supplementary information The online version contains supplementary material available at <https://doi.org/10.1038/s43247-025-02018-5>.

Correspondence and requests for materials should be addressed to Philipson Bani.

Peer review information *Communications Earth & Environment* thanks Michelle Muth and the other, anonymous, reviewer(s) for their contribution to the peer review of this work. Primary Handling Editor: Carolina Ortiz Guerrero. A peer review file is available.

Reprints and permissions information is available at <http://www.nature.com/reprints>

Publisher's note Springer Nature remains neutral with regard to jurisdictional claims in published maps and institutional affiliations.

Open Access This article is licensed under a Creative Commons Attribution-NonCommercial-NoDerivatives 4.0 International License, which permits any non-commercial use, sharing, distribution and reproduction in any medium or format, as long as you give appropriate credit to the original author(s) and the source, provide a link to the Creative Commons licence, and indicate if you modified the licensed material. You do not have permission under this licence to share adapted material derived from this article or parts of it. The images or other third party material in this article are included in the article's Creative Commons licence, unless indicated otherwise in a credit line to the material. If material is not included in the article's Creative Commons licence and your intended use is not permitted by statutory regulation or exceeds the permitted use, you will need to obtain permission directly from the copyright holder. To view a copy of this licence, visit <http://creativecommons.org/licenses/by-nc-nd/4.0/>.

© The Author(s) 2025